Proceedings of the ASME 2016 International Mechanical Engineering Congress and Exposition
IMECE2016
November 11-17, 2016, Phoenix, Arizona, USA

IMECE2016-66696

A COMPONENT-WISE APPROACH TO ANALYSE A COMPOSITE LAUNCHER STRUCTURE SUBJECTED TO LOADING FACTOR

Tommaso Cavallo*, Alfonso Pagani, Enrico Zappino, Erasmo Carrera
Department of Mechanical and Aerospace Engineering
Politecnico di Torino
C.so Duca degli Abruzzi 24, 10029, Turin, Italy

ABSTRACT

The space structures are realized by combining skin and reinforced components, such as longitudinal reinforcements called stringers and transversal reinforcements called ribs. These reinforced structures allow two main design requirements to be satisfied, the former is the light weight and the latter is a high strength. Solid models (3D) are widely used in the Finite Element Method (FEM) to analyse space structures because they have a high accuracy, in contrast they also have a high number of degrees of freedoms (DOFs) and huge computational costs. For these reasons the one-dimensional models (1D) are gaining success as alternative to 3D models. Classical models, such as Euler-Bernoulli or Timoshenko beam theories, allow the computational cost to be reduced but they are limited by their assumptions. Different refined models have been proposed to overcome these limitations and to extend the use of 1D models to the analysis of complex geometries or advanced materials. In this work very complex space structures are analyzed using 1D model based on the Carrera Unified Formulation (CUF). The free-vibration analysis of isotropic and composite structures are shown. The effects of the loading factor on the natural frequencies of an outline of launcher similar to the Arian V have been investigated. The results highlight the capability of the present refined one-dimensional model to reduce the computational costs without reducing the accuracy of the analysis.

*Corresponding author e-mail:tommaso.cavallo@polito.it

INTRODUCTION

One-dimensional models are widely used in the engineering field because these models make it possible to reduce the DOFs and the computational costs as a first consequence. The use of 1D and 2D refined elements can reduce the computational costs but also the accuracy of the solution. These models are based on classical structural theories, Euler-Bernoulli [1] or Timoshenko [2] in the 1D models, Love-Kirchhoff [3] or Reissner-Mindlin [4] in the 2D models. These classical finite elements show the same limitations of the theoretical models on which are based. 2D elements are not able to describe the shear stresses accurately, and the analysis of laminated plates can be not accurate. 1D elements do not consider the cross-sectional deformation, therefore, when they are used as stringers, the local modes can not be accounted for. Refined 1D and 2D structural models can improve the accuracy of the solutions with respect to the classical models with a lower computational cost than the three-dimensional models.

A step forward in the development of refined structural models has been done with the introduction of the Carrera Unified Formulation (CUF) [5], a mathematical tool able to derive high-order models in a compact form. The use of the component-wise (CW) approach [6] makes it possible to study very complex structures using a unique 1D formulation, for both static [7] and dynamic [8] analyses. In the present paper, different complex space structures have been analyzed using the CW approach. The free-vibration analyses of complex structures have been performed to highlight the capabilities of the 1D-refined models based on the CUF. Both isotropic and composite material have been considered. The analysis of a launcher structure has been

finally proposed In addition a focus on the results about an outline of launcher are proposed. The launcher considered has a shape similar to the European launcher Arian V composed by a central body and two lateral boosters. The results are compared with respect to the results from the 3D refined model analyzed using the commercial software NASTRAN, and they highlight the accuracy of the model proposed in terms of results and DOFs obtained.

Refined one-dimensional models

Figure 1 shows the adopted coordinate frame, where the $y-axis$ is the beam axis and its ranges from 0 to L, where L is the total length of the beam. The symbol Ω denotes the cross-section of the beam. The transposed displacement vector can be written

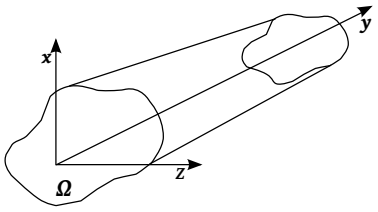

FIGURE 1. Reference system for the 1D CUF Model

as:

$$\mathbf{u}(x,y,z) = \left\{ u_x \; u_y \; u_z \right\}^T \tag{1}$$

u_x, u_y and u_z are the three components of the displacement vector $\mathbf{u}(x,y,z)$. The superscript T denotes transposition. The stress, σ, and the strain, ε, can be written using the following formulation:

$$\sigma^T = \left\{ \sigma_{xx} \; \sigma_{yy} \; \sigma_{zz} \; \sigma_{xy} \; \sigma_{xz} \; \sigma_{yz} \right\} \tag{2}$$

$$\varepsilon^T = \left\{ \varepsilon_{xx} \; \varepsilon_{yy} \; \varepsilon_{zz} \; \varepsilon_{xy} \; \varepsilon_{xz} \; \varepsilon_{yz} \right\} \tag{3}$$

Strain can be derived from the displacements using the classical linear geometrical equation:

$$\varepsilon = \mathbf{D}\mathbf{u} = \left([\mathbf{D}_y] + [\mathbf{D}_\Omega] \right) \mathbf{u} \tag{4}$$

Where $\mathbf{D}$ is a differential operator [9]. $\mathbf{D}_y$ and $\mathbf{D}_\Omega$ represent the differential operator on the beam axis y and on the beam cross-section, respectively. The Hooke's law of the material, if considered isotropic, can be written as:

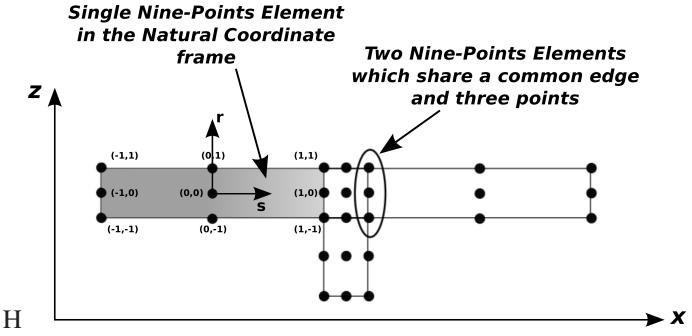

FIGURE 2. Cross-section discretization and assembly with the $L9$ elements.

$$\sigma = \mathbf{C}\varepsilon \tag{5}$$

Lagrange Polynomials

In the 1D problem, the displacement field $\mathbf{u}$ can be written as the product of two functions, a cross-sectional expansion function, called F_τ, and the generalized displacement vector unknown on the beam axis, $\mathbf{u}_\tau$:

$$\mathbf{u}(x,y,z) = F_\tau(x,z)\mathbf{u}_\tau(y) \tag{6}$$

where τ can range from 1 to the number of points of the single element used on the cross-section, four-points ($L4$) or nine-points ($L9$) elements can be adopted. The isoparametric formulation is exploited to deal with arbitrary cross-section shaped geometries. In this work, the nine-points elements are used and their interpolation functions are:

$$\begin{aligned} F_\tau &= \tfrac{1}{4}(r^2 + r\, r_\tau)(s^2 + s\, s_\tau) \qquad \tau = 1,3,5,7 \\ F_\tau &= \tfrac{1}{2}s_\tau^2(s^2 - s\, s_\tau)(1-r^2) + \tfrac{1}{2}r_\tau^2(r^2 - r\, r_\tau)(1-s^2) \qquad \tau = 2,4,6,8 \\ F_\tau &= (1-r^2)(1-s^2) \qquad \tau = 9 \end{aligned} \tag{7}$$

Where the indexes r and s range from -1 to $+1$. Fig.2 shows as many $L9$ elements can be assembled in order to build complex cross-section.

In the present work the models based on the Lagrange expansion will be named as LE models.

Finite Element Solution

The displacement field along the $y-axis$ is approximated using the Finite Element Method (FEM). The generalized displacement vector, $u_\tau(y)$, is linearly interpolated using the classical shape functions. N_{NE} is the number of the nodes of a beam

element along the axis. The generalized displacement vector becomes:

$$\mathbf{u}_\tau(y) = N_i(y)\mathbf{q}_{i\tau}; \quad i = 1 \dots N_{NE} \tag{8}$$

Therefore, the displacement field can be written as follows:

$$\mathbf{u}(x,y,z) = F_\tau(x,z)N_i(y)\mathbf{q}_{i\tau} \tag{9}$$

Where with the index i is indicated the node of the element along the beam axis. The three-nodes ($B3$) refined beam elements are used along the beam axis in the present work as shown in Fig.3. Figure 3 shows an example of a thin-walled beam which uses

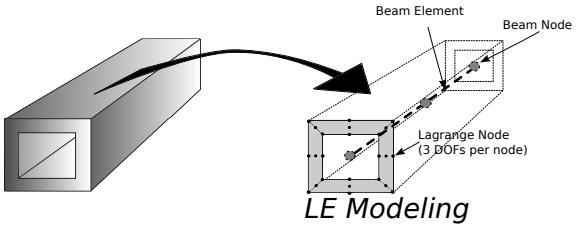

FIGURE 3. Example of a LE modelling and beam configuration

four L9 element over the cross-section and two beam element along the longitudinal axis.

The Component-Wise Approach

The component-wise approach makes it possible to model each structural element singularly.

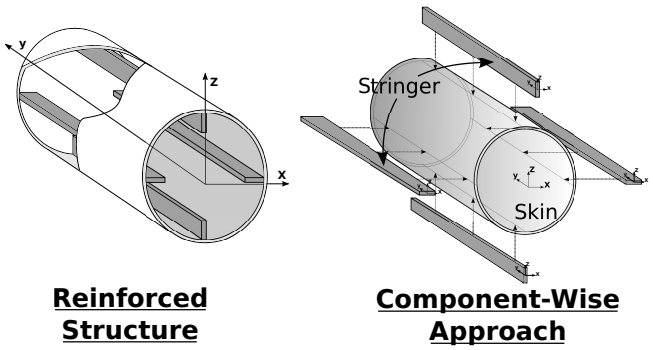

FIGURE 4. Reinforced structure assembled using the Component-Wise approach.

Figure4 shows a reinforced structure made by a thin-walled cylinder reinforced with four stringer. Using the CW approach each component, the stringers and the skin, is intended as an independent beam model, the different parts can be assembled in a unique structural model during the assembly procedure. More details about the *LE* model and the CW approach can be found in subsequent section and in [6, 10, 11]

Governing Equation

The governing equations are derived via the Principle of Virtual Displacements (PVD) that in the dynamic case assumes the following form:

$$\delta L_{int} = \delta L_{ext} - \delta L_{ine} \tag{10}$$

Where L_{int} stands for the strain energy, L_{ext} is the work of the external loadings, and L_{ine} is the work of the inertial loadings. δ denotes the virtual variation. Considering the free vibration analysis, the external work is equal to zero and the Eq.10 becomes:

$$\delta L_{int} + \delta L_{ine} = 0 \tag{11}$$

The internal work can be written as:

$$\delta L_{int} = \int_V \delta\varepsilon^T \sigma dV \tag{12}$$

Using the constitutive equations and the geometrical relations given respectively in Eq.4 and Eq.5 and introducing the displacement field given in Eq. 9, the variation of the internal work becomes:

$$\delta L_{int} = \delta \mathbf{q}_{\tau i}^T \int_V \left[N_i(y)F_\tau(x,z)\ \mathbf{D}^T\ \mathbf{C}\ \mathbf{D}\ F_s(x,z)N_j(y)\right] dV \mathbf{q}_{sj} = \delta \mathbf{q}_{sj}^T \mathbf{K}^{ij\tau s}\mathbf{q}_{\tau i} \tag{13}$$

The $\mathbf{D}$ matrix operates on the functions F_τ, F_s, N_i and N_j. $\mathbf{K}^{ij\tau s}$ is the stiffness matrix written in form of "*fundamental nucleus*" that is a 3×3 matrix. $\mathbf{q}_{\tau i}$ is the vector of the nodal unknown and $\delta\mathbf{q}_{sj}$ is its virtual variation. In the end $\mathbf{I}$ is the identity matrix. The virtual variation of the work of the inertial loadings can be written as following:

$$\delta L_{ine} = \int_V \delta\mathbf{u}^T\ \rho\ \ddot{\mathbf{u}}\ dV \tag{14}$$

where $\ddot{\mathbf{u}}$ means the acceleration vector and ρ stands the density of the material. The Eq.14 can be rewritten using Eq.4:

$$\delta L_{ine} = \delta \mathbf{q}_{sj}^T \int_l N_i(y) \left\{ \int_\Omega \rho \left[F_\tau(x,z)\ \ \mathbf{I}\right] \left[F_s(x,z)\ \ \mathbf{I}\right] d\Omega \right\} N_j(y) dz \ddot{\mathbf{q}}_{\tau i}$$
$$= \quad \delta \mathbf{q}_{sj}^T\ \mathbf{M}^{ij\tau s}\ \ddot{\mathbf{q}}_{\tau i} \tag{15}$$

$\mathbf{M}^{ij\tau s}$ is the 3×3 mass matrix in the form of *fundamental nucleus*, the indices have the same meaning of those of stiffness matrix. The explicit form of the fundamental nucleus for both the stiffness and the mass matrices can be found in [9]. In conclusion, the PVD can be written as following:

$$\delta \mathbf{q}_{sj}^T \left(\mathbf{K}^{ij\tau s}\ \mathbf{q}_{\tau i} + \mathbf{M}^{ij\tau s}\ \ddot{\mathbf{q}}_{\tau i} \right) = 0 \tag{16}$$

The global stiffness and mass matrices are obtained by means of the classical FE assembling procedure, as shown in [9]. The equation can be written as:

$$\boldsymbol{M}\ddot{\boldsymbol{q}} + \boldsymbol{K}\boldsymbol{q} = 0 \tag{17}$$

Where $\boldsymbol{q}$ is the global unknowns vector. Due to the linearity of the problem an harmonic solution is considered and the natural frequencies, ω_k, are obtained by solving the following eigenvalues problem:

$$\left(-{\omega_k}^2 \boldsymbol{M} + \boldsymbol{K} \right) \boldsymbol{q}_k = 0 \tag{18}$$

Where $\boldsymbol{q}_k$ is the *k-th* eigenvector, and k ranges form 1 to total numbers of DOF of the structures.

Load factor formulation

When structures undergo to strong accelerations, the effects of the inertial loading factors may afflict strongly the dynamic response of the structures, as shown in the [12, 13]. The effects of these loads can be included in the formulation presented in the previous section considering the effect of the load factor as an external load.

The acceleration applied to the structure can be written as:

$$\ddot{u}_0 = \left(\ddot{u}_{x_0}, \ddot{u}_{y_0}, \ddot{u}_{z_0} \right)^T \tag{19}$$

The external work due to the acceleration can be written as:

$$\delta L_{ext} = \int_V \rho\, \delta \mathbf{u}^T \ddot{\mathbf{u}}_0 dV \tag{20}$$

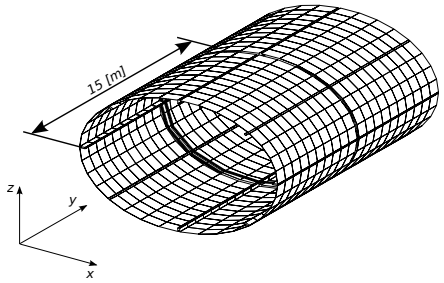

FIGURE 5. Reinforced Cylinder Model.

Using the notation introduced before, the external work due to the inertial loads can be written as:

$$\delta L_{ext} = \delta \mathbf{q}_{js}^T \mathbf{M}^{ij\tau s} \mathbf{q}_{i\tau_0} = \delta \mathbf{q}_{js}^T \mathbf{P}_{ine}^{js} \tag{21}$$

where $\mathbf{P}_{ine}^{js}$ is the loading vector due to the inertial load.

Numerical Assessment

This section investigates the behavior of the CUF models in the analysis of very complex reinforced structure. In this work the CUF models are called *LE* models. The free-vibration analysis of two different structures is considered. The first structure analyzed is a reinforced cylinder made using both isotropic and composite materials, while the second component is an outline of launcher characterized by a central body and two lateral boosters. All structures are reinforced using longitudinal and transversal stringers. Two solid FE models are made using the commercial code MSC NASTRAN. They are called *Solid* (3*D*) model and *Shell* $-$ *beam* ($2D-1D$) model. The 3*D* model is build using only solid elements, while the $2D-1D$ are made using the 2D elements for the skin and the beam element for the stringers and ribs. in the second case the use of the correct offset is mandatory in order to represent properly the geometry of the structure, The 3*D* model is used as reference model to compare the results.

Reinforced cylinder

The geometrical properties of the structure and of the cross-section are shown in the Fig.5 and Fig.6, respectively. Between two stringers there are two nine-nodes elements, while for each stringer only one nine-nodes element is used and one nine-nodes element is used to connect each stringer to the skin. In total 32 nine-nodes elements are used on the cross-section.

The structure is clamped at both ends. Three components are assembled to build the whole structure using the component-wise approach . Figure 7 shows the beam configuration, where the components 1 and 3 have the same cross-section (Figure 6a).

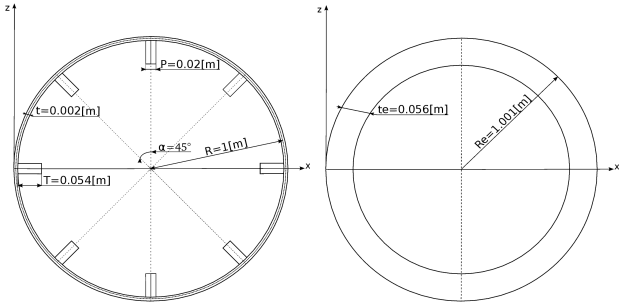

(a) *Component* 1 *and* 3. (b) *Component* 2.

FIGURE 6. Cross-Section Geometry.

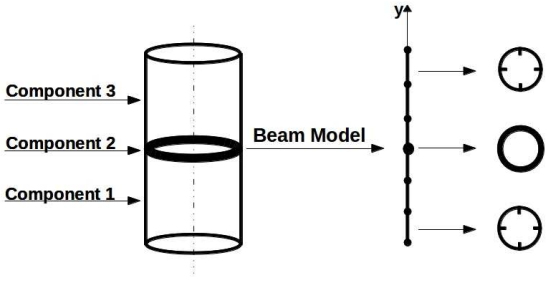

FIGURE 7. Component-Wise Approach.

The components 1 and 3 are thin-walled cylinders reinforced using eight stringers while the component 2 (Figure 6b) is a circumferential reinforcement, a rib. The $B3$ refined beam elements are used along the $y-axis$ for all the three components. In particular four $B3$ are used for the component one and three, and 1 $B3$ component for the second component.

Isotropic Structure The structure is made of aluminium with a value of Young modulus, E, equal to 75 GPa, the Poisson ratio, ν, equal to 0.3 and the value of density, ρ equal to 2700 kg/m^3. The first two bending and torsional frequencies, computed using different structural models, are shown in Tab.1. The refined mesh as been used to build the solid model and therefore the $3D$ results are used as reference and they are shown in the first column. The mixed one- and two-dimensional FE model allows the number of DOFs to be drastically reduced but in the case of the first bending and torsional frequencies shows an error greater than 10%. These differences can be due to the geometrical approximations introduced by the classical FEM modelling. In fact the reinforcements are considered as beams placed on the skin reference surface, an appropriate offset has been used in order to represent properly the mass and stiffness distribution. The results obtained using the present *LE* model are very close with respect to the reference solution. The LE model is able to represent the real geometry of the structure without introduce any approximation and without the use of offset. In the case of the bending frequencies (see Fig.8)the error is lower than the 2% while, when the torsional frequencies are considered the error is still lower than 10%. The DOFs of the $LE_{isotropic}$ are about the 2% than the $3D$ while the FEM_{2D-1D} DOFs are about the 7%.

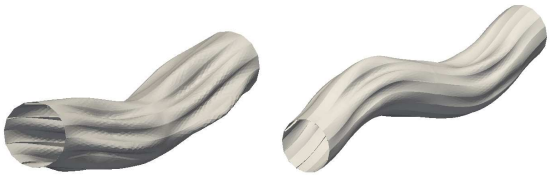

(a) $F_1 = 34.23[Hz]$. (b) $F_2 = 93.85[Hz]$.

FIGURE 8. First and second bending frequencies of $LE_{isotropic}$ model.

TABLE 1. Comparisons of the first two bending and torsional frequencies of the reinforced cylinder using different structural model [Hz].

$Mode$	FEM_{3D}	FEM_{2D-1D}	$LE_{isotropic}$
DOF :	390192	26206	8352
Bending	Frequencies:		
1^a	33.64	37.49 $^{(+11.4\%)}$	34.23 $^{(+1.7\%)}$
2^a	94.82	91.06 $^{(-4.0\%)}$	93.85 $^{(-1.0\%)}$
Torsion	Frequencies:		
1^a	67.67	77.83 $^{(+15.0\%)}$	73.18 $^{(+8.1\%)}$
2^a	175.33	179.49$^{(+2.4\%)}$	174.61$^{(-0.4\%)}$

$(\,)^{(*\%)}$: $*$ *Percentage difference with respect to the* 3*D FE Model*

Composite Structure The geometry of the composite structures is the same as shown in the Fig.5 and Fig.6, such as the beam configuration shown in Fig.7. In this case, the thin-walled skin has been built using a composite material while the ribs and the stringers are made using the same isotropic material used before. Table 2 shows the properties of the composite material used. In these components, the fibers have different orientations as shown in Fig.9, a two layers (+45/-45) lamination has been used.

Table 3 shows the results of the composite model with respect to the isotropic model. The use of the composite material has increased mostly the torsional frequencies than the bending frequency. In fact, while the bending stiffness is mainly due to the reinforcements, that are still built in aluminum, the torsional

TABLE 2. Component-Wise Approach.

Orthotropic	*Material*
E_{33}	142 [MPa]
$E_{22} = E_{11}$	9.8 [MPa]
$G_{32} = G_{31}$	6 [MPa]
G_{21}	4.83 [MPa]
$\nu_{32} = \nu_{31}$	0.42
ν_{21}	0.45
ρ	1445 $[kg/m^3]$

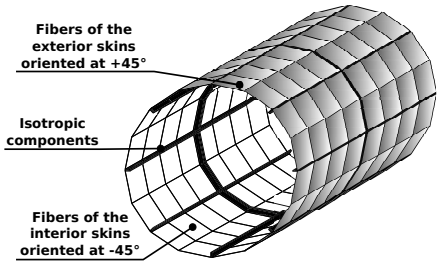

FIGURE 9. Composite cylinder materials set-up.

stiffness is mainly due to the skin. That is, the use of composite material in the skin may increase the torsional frequencies, as shown by the results.

TABLE 3. Effect of the composite material on the frequencies.

Mode	$LE_{isotropic}$	$LE_{composite}$
DOF :	8352	16848
Bending	Frequencies:	
1^a	34.23	34.16 $^{(-0.3\%)}$
2^a	93.85	101.31 $^{(+7.9\%)}$
Torsion	Frequencies:	
1^a	73.18	90.90 $^{(+24.2\%)}$
2^a	174.61	283.49$^{(+62.3\%)}$

Launcher Structure

The shape of the launcher used in the present section is similar to the European launcher *Arian V* developed by the European Space Agency, ESA. The geometry is shown in Figure 10, it is

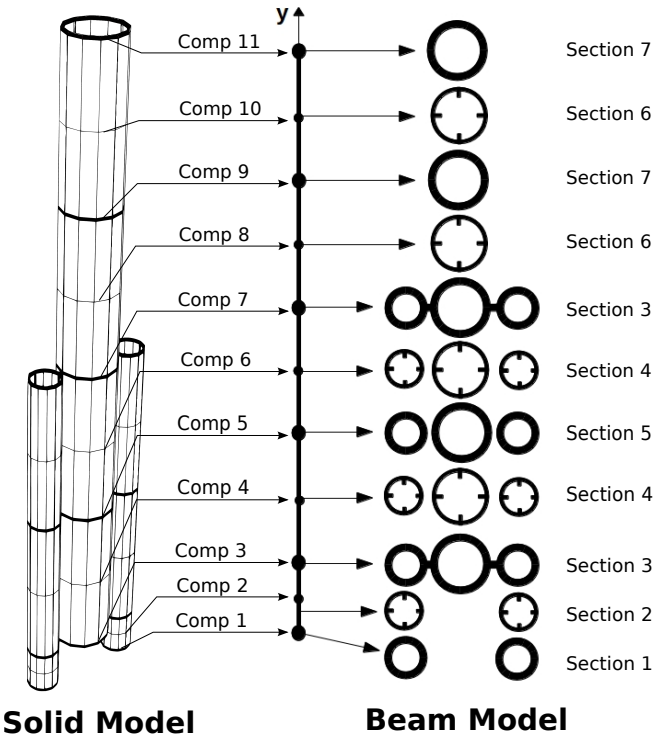

FIGURE 10. Launcher structure

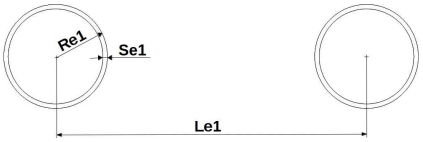

FIGURE 11. Section 1

characterized by three main bodies, the central body used for the cryogenic fuel and the payload and two lateral boosters where the solid fuel is stored. The structure is made of aluminum with a value of Young modulus, E, equal to 75 GPa, the Poisson ratio, ν, equal to 0.3 and the value of density, ρ, equal to 2700 kg/m^3.

The beam configuration is shown in Fig.10 where the seven main longitudinal sections are highlighted. In sections 1, 3, 5 and 7 only one *B*3 is used, while the other sections are modelled using two B3 elements. Figures 11, 12, 13, 14, 15, 16 and 17 show the 7 different cross-sections used to build the model, with their geometrical properties reported in Table 4.

Two *Solid* FE models have been used to compare the results. The main $Refined\ FE-3D$ model has refined mesh that a high number of degrees of freedom (DOFs), equal to 197436. The other $FE-3D$ model has been built having the same number of DOFs than the *LE* model, equal to 29628.

The correspondences between the *LE* model and the

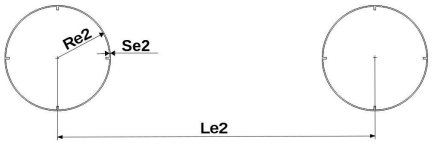

FIGURE 12. Section 2

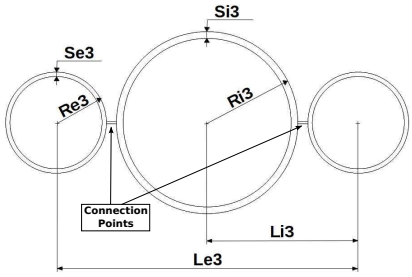

FIGURE 13. Section 3

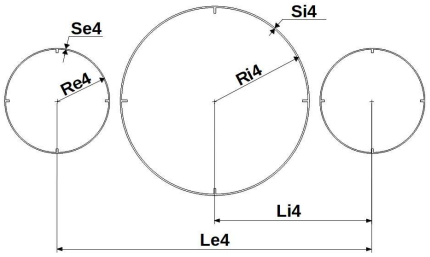

FIGURE 14. Section 4

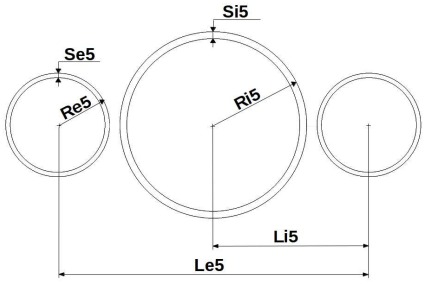

FIGURE 15. Section 5

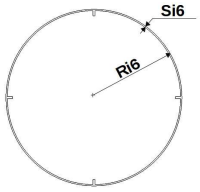

FIGURE 16. Section 6

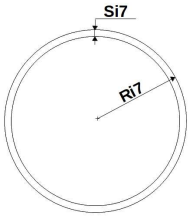

FIGURE 17. Section 7

TABLE 4. Geometrical data of the launcher structure

ID Sec	*Comp*	$Cross-Section\ [m]$	$Lenght\ [m]$
1 (Fig.11)	1	$Re_1 = 1.50$	$h = 0.25$
		$Se_1 = 0.13$	
		$Le_1 = 9.00$	
2 (Fig.12)	2	$Re_2 = 1.50$	$h = 3.50$
		$Se_2 = 0.03$	
		$Le_2 = 9.00$	
3 (Fig.13)	3 / 7	$Re_3 = 1.50$ $Ri_3 = 2.70$	$h = 0.25$
		$Se_3 = 0.13$ $Si_3 = 0.20$	
		$Le_3 = 9.00$ $Li_3 = 4.50$	
4 (Fig.14)	4 / 6	$Re_4 = 1.50$ $Ri_4 = 2.70$	$h = 13.50$
		$Se_4 = 0.03$ $Si_4 = 0.04$	
		$Le_4 = 9.00$ $Li_4 = 4.50$	
5 (Fig.15)	5	$Re_5 = 1.50$ $Ri_5 = 2.70$	$h = 0.25$
		$Se_5 = 0.13$ $Si_5 = 0.20$	
		$Le_5 = 9.00$ $Li_5 = 4.50$	
6 (Fig.16)	8 / 10	$Ri_6 = 2.70$	$h = 13.50$
		$Si_6 = 0.04$	
7 (Fig.17)	9 / 11	$Ri_7 = 2.70$	$h = 0.25$
		$Si_7 = 0.20$	

h : *Component size along the* $y-axis$

$Refined\ FE-3D$ model, and between the $FE-3D$ model and the $Refined\ Solid$ model is further investigated by means of the Modal Assurance Criterion (MAC), which is represented graphically in Figure 18a and Figure 18b, respectively.

The MAC is defined as a scalar representing the degree of consistency (linearity) between two modes (see Ref.22) as follows:

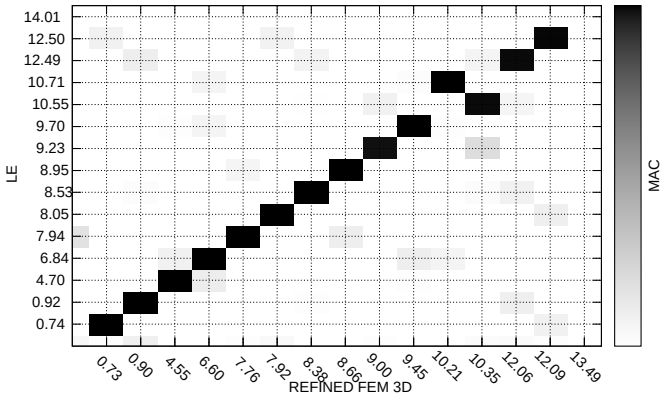

(a) *LE Model Vs Refined FE3D Model.*

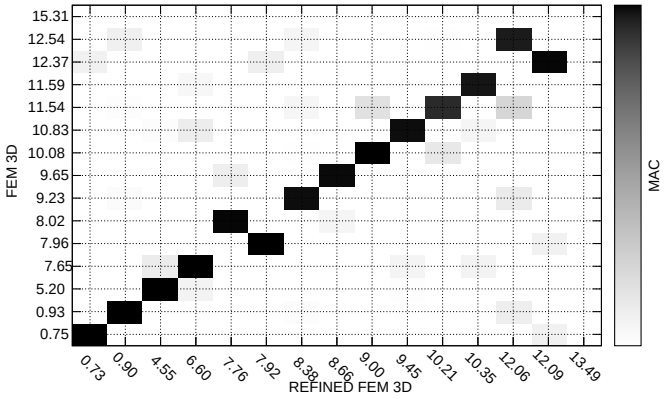

(b) *FE3D Model Vs Refined FE3D Model.*

FIGURE 18. Comparison of first 15 no rigid modes using the MAC.

$$MAC_{ij} = \frac{\left|\{\phi_{A_i}\}^T\{\phi_{B_j}\}\right|^2}{\{\phi_{A_i}\}^T\{\phi_{A_i}\}\{\phi_{B_j}\}\{\phi_{B_j}\}^T} \tag{22}$$

where, $\{\phi_{A_i}\}$ is the i^{th}-eigenvector of model A, while $\{\phi_{B_j}\}$ is the j^{th}-eigenvector of model B. The MAC can range from zero (no correspondence with white block) to 1 (full correspondence with a full black block). When there are same blocks with different tonalities of gray, it means that there are different similar modes and, in this case, the best dark block is considered.

Figure 18a shows how for the first ten modes, there is an almost perfect matching between the LE model and the $Refined\ FE-3D$ model.

In contrast, Fig18b shows how there is no a perfect matching between mode 5 and mode 6 when the $FE-3D$ model and the $Refined\ FE-3D$ model are considered. In particular mode 5 of the $FE-3D$ model is mode 6 of the $Refined\ FE-3D$ mode, at the same way mode 6 of the $FE-3D$ model is mode 5 of the $Refined\ FE-3D$ mode.

TABLE 5. First 14 Modes in [Hz] for empty Launcher.

MODE	$REF\ FEM-3D$	$FEM-3D$	LE
DOF	197436	29628	29628
1	0.73	0.75 $^{(+2.7\%)}$	0.74 $^{(+1.4\%)}$
2	0.90	0.93 $^{(+3.3\%)}$	0.92 $^{(+2.2\%)}$
3	4.55	5.20 $^{(+14.3\%)}$	4.70 $^{(+3.3\%)}$
4	6.60	7.65 $^{(+15.9\%)}$	6.84 $^{(+3.6\%)}$
5	7.76	8.02 $^{(+3.4\%)}$	7.94 $^{(+2.3\%)}$
6	7.92	7.96 $^{(+0.5\%)}$	8.05 $^{(+1.6\%)}$
7	8.38	9.23 $^{(+10.1\%)}$	8.53 $^{(+1.8\%)}$
8	8.66	9.65 $^{(+11.4\%)}$	8.95 $^{(+3.3\%)}$
9	9.00	10.08 $^{(+12.0\%)}$	9.23 $^{(+2.6\%)}$
10	9.45	10.83 $^{(+14.6\%)}$	9.70 $^{(+2.6\%)}$
11	10.21	11.54 $^{(+13.0\%)}$	10.71 $^{(+4.9\%)}$
12	10.35	11.59 $^{(+12.0\%)}$	10.55 $^{(+1.9\%)}$
13	12.06	12.54 $^{(+4.0\%)}$	12.49 $^{(+3.6\%)}$
14	12.09	12.37 $^{(+2.3\%)}$	12.50 $^{(+3.4\%)}$

$(\ )^{(*\%)} : *$ *percentage difference with respect to refined FE3D Model*

Table 5 shows that the best correspondence with the $Refined\ FE-3D$ model is obtained when the LE model is used. In this case, the error of the LE model is lower than the 5% for the modes considered and the LE DOFs are only the 15% of those used in the $Refined\ FE-3D$.

Figure 19 shows the first 9 modes of the LE model. The local modes of the boosters are highlighted in the Figures 19a and b. Figures 19c and d show the global shell-like modes and Fig.19e shows the bending mode in the central body and the shell-like mode that involves the two boosters. The first bending mode appears in the Fig.19f.

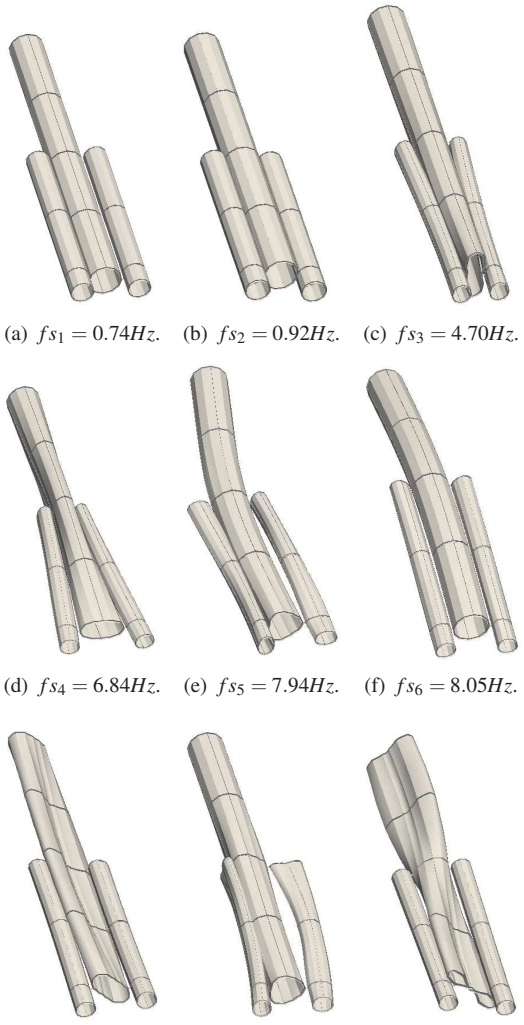

(a) $fs_1 = 0.74Hz$. (b) $fs_2 = 0.92Hz$. (c) $fs_3 = 4.70Hz$.

(d) $fs_4 = 6.84Hz$. (e) $fs_5 = 7.94Hz$. (f) $fs_6 = 8.05Hz$.

(g) $fs_7 = 8.53Hz$. (h) $fs_8 = 8.95Hz$. (i) $fs_8 = 9.23Hz$.

FIGURE 19. First 9 Modes for the *LE* Model

1 Concluding Remarks

In this work, different finite element models have been compared in the free vibration analysis of complex reinforced structures. In particular, a reinforced cylinder structure was analyzed, and a sample launcher was studied. Metallic and composite materials have been considered. Different one-dimensional refined models were derived using the Carrera Unified Formulation based on the Lagrange expansion. In addition, different FE models derived using the commercial code NASTRAN were used to compare the results. Considering the results obtained by the analyses performed, it can be concluded that:

1. the 1D CUF models overcome the limitation of the classical one-dimensional models, they allow the global modes and local (shell like) modes to be detected;
2. the component-wise approach used in the present refined 1D model permits to analyse both thin-walled structures and reinforced components using the same element;
3. the refined 1D LE models used in the present work can reduce the number of degrees of freedom preserving the accuracy of the solution.

In conclusion, the models herein used can very attractive for the analysis of different reinforced structures. It can be used in the analysis of complex structures, and advanced material can be considered.

REFERENCES

[1] Euler, L., 1744. *De curvis elasticis. methodus inveniendi lineas curvas maximi minimive proprietate gaudentes, sive solutio problematis iso-perimetrici lattissimo sensu accepti*. Bousquet, Geneva.

[2] Timoshenko, S. P., 1959. *Theory of Plates and Shells, 2nd ed.* New York.

[3] Kirchhoff, G., 1959. "Uber das gleichgwich und die bewegung einer elastischen schiebe". *J. Angew. Math.,* ***40***, pp. 51 – 88.

[4] Reissner, E., 1945. "The effect of transverse shear deformation on the bending of elastic plates". *ASME Journal of Applied Mechanics,* ***12***, pp. 68 – 77.

[5] Carrera, E., Cinefra, M., Petrolo, M., and Zappino, E., 2014. *Finite Element Analysis of Structures Through Unified Formulation*.

[6] Carrera, E., Pagani, A., and Petrolo., M., 2013. "Classical, refined and component-wise analysis of reinforced-shell structures". *AIAA Journal,* ***51***, pp. 1255 – 1268.

[7] Carrera, E., Zappino, E., and Cavallo, T., 2016. "Static analysis of reinforced thin-walled plates and shells by means of various finite element models". *International Journal for Computational Methods in Engineering Science & Mechanics*. In press.

[8] Carrera, E., Zappino, E., and Cavallo, T., 2015. "Accurate free vibration analysis of launcher structures using refined 1d model". *International Journal of Aeronautical and Space Sciences (IJASS),* ***16***, pp. 206 – 222.

[9] Carrera, E., Cinefra, M., Petrolo, M., and Zappino, E., 2014. *Finite Element Analysis of Structures Through Unified Formulation*. John Wiley & Sons.

[10] Carrera, E., Pagani, A., and Petrolo, M., 2013. "Component-wise method applied to vibration of wing structures". *JOURNAL OF APPLIED MECHANICS,* ***80***(4), pp. 041012–1–041012–15.

[11] Carrera, E., and Pagani, A., 2014. "Free vibration analysis of civil engineering structures by component-wise models". *JOURNAL OF SOUND AND VIBRATION,* ***333***, pp. 4597–4620.

[12] Carrera, E., Pagani, A., and Zangallo, F., 2014. "Thin-

walled beams subjected to load factors and non-structural masses". *INTERNATIONAL JOURNAL OF MECHANICAL SCIENCES,* ***81***, pp. 109–119.

[13] Carrera, E., and Pagani, A., 2016. "Accurate response of wing structures to free-vibration, load factors and non-structural masses". *AIAA JOURNAL,* ***54***(1), pp. 227–241.